

# Chemical characterization of organic compounds involved in iodine-initiated new particle formation from coastal macro-algal emission

Yibei Wan<sup>1</sup>, Xiangpeng Huang<sup>2</sup>, Chong Xing<sup>1</sup>, Qiongqiong Wang<sup>1</sup>, Xinlei Ge<sup>2</sup>, Huan Yu<sup>1,\*</sup>

<sup>1</sup> School of Environmental Studies, China University of Geosciences, Wuhan, 430074, China

<sup>2</sup> Jiangsu Key Laboratory of Atmospheric Environment Monitoring and Pollution Control, Collaborative Innovation Center of Atmospheric Environment and Equipment Technology, School of Environmental Science and Engineering, Nanjing University of Information Science and Technology, Nanjing 210044, China

\* To whom correspondence should be addressed: yuhuan@cug.edu.cn

## Abstract

Iodine-initiated new particle formation (I-NPF) has long been recognized in coastal hotspot regions. However, no prior work has studied the exact chemical composition of organic compounds and their role in the coastal I-NPF. Here we present an important complementary study to the ongoing laboratory and field researches of iodine nucleation in coastal atmosphere. Oxidation and NPF experiments with vapor emissions from real-world coastal macroalgae were simulated in a bag reactor. On the basis of comprehensive mass spectrometry measurements, we reported for the first time a variety of volatile precursors and their oxidation products in gas and particle phases in such a highly complex system. Organic compounds overwhelmingly dominated over iodine in the new particle growth initiated by iodine species. The identity and transformation mechanisms of organic compounds were identified in this study to provide a more complete story of coastal NPF from low-tide macroalgal emission.

## 1. Introduction

Coastal new particle formation (NPF) may be driven by daytime low-tide emission of iodine species from macroalgae fully or partially exposed to the air. The phenomenon was reported in hotspot locations of west Europe, Australia and polar regions (Allan et al., 2015; Baccharini et al., 2020; Beck et al., 2021; Heard et al., 2006; McFiggans et al., 2010; O'Dowd et al., 2002; Sipil äet al., 2016; Whitehead et al., 2009). In the southeast coastline of China, we reported intense iodine-initiated NPF based on particle number size distribution and iodine measurements (Yu et al.,

32 2019).

33 To simulate iodine-initiated NPF (I-NPF) in controlled laboratory conditions, I<sub>2</sub> or CH<sub>2</sub>I<sub>2</sub> vapor  
34 was usually photolyzed in the presence of ozone to provide nucleation precursors (Burkholder et al.,  
35 2004; He et al., 2021; Huang et al., 2022; Jimenez et al., 2003; Martín et al., 2020; Monahan et al.,  
36 2012; O'Dowd et al., 2004; Saunders and Plane, 2005). Ashu-Ayem et al. (2012); McFiggans et al.  
37 (2004); Monahan et al. (2012); Sellegri et al. (2005) and Sellegri et al. (2016) also investigated the  
38 NPF from the vapors emitted by real-world macroalgal specimens or seawater in laboratory chamber  
39 or apparatus. However, the focus of all above studies are emission rate, oxidation mechanisms or  
40 nucleation pathways of iodine species. For example, positive correlations between particle  
41 concentrations and I<sub>2</sub> or CH<sub>2</sub>I<sub>2</sub> mixing ratios were usually observed (Burkholder et al., 2004; Jimenez  
42 et al., 2003; Monahan et al., 2012; Sellegri et al., 2005). Kinetic studies in flow tube or CERN  
43 CLOUD chamber proposed the clustering of iodine oxides (I<sub>x</sub>O<sub>y</sub>) or iodine oxoacids (HIO<sub>3</sub>, HIO<sub>2</sub>) as  
44 nucleation mechanisms on the basis of photoionization TOF-MS (Martín et al., 2020), Api-TOF and  
45 nitrate-Chemical Ionization Mass Spectrometer (CIMS) measurements (He et al., 2021). A recent  
46 chamber study showed heterogeneous reaction between iodine oxide nanoparticle, meso-erythritol  
47 (or glyoxal) and dimethylamine accelerated nanoparticle growth (Huang et al., 2022).

48 Until now, no prior work has investigated the exact chemical identity of organic compounds  
49 (other than iodinated methane) and their role in I-NPF. The role of biogenic terpenes and  
50 anthropogenic aromatics in continental NPF has been recognized for a long time (Donahue et al.,  
51 2013). Their ozonolysis or photochemistry products have been investigated in depth by using  
52 Electrospray Ionization Mass Spectrometry (ESI-MS) and more recently, CIMS (Ehn et al., 2014;  
53 Faxon et al., 2018; Kundu et al., 2012; Kundu et al., 2017; Nguyen et al., 2010; Riva et al., 2017;  
54 Wang et al., 2020; Yan et al., 2020). It is very likely that certain volatile organic compounds (VOCs)  
55 emitted mutually with iodine or iodinated methane from coastal biota or biologically active sea  
56 surface may also be involved in coastal I-NPF process and promote the growth of iodine particles.

57 To test this hypothesis, we conducted oxidation and NPF experiments with vapor emissions from  
58 real-world coastal macroalgae in a bag reactor. A suite of mass spectrometric methods including  
59 Inductively Coupled Plasma-MS (ICP-MS), Gas Chromatography-MS (GC-MS), iodide-CIMS and  
60 ESI-orbitrap MS were applied to measure vapor precursors, gaseous products and particulate  
61 products during the NPF process. Mass concentrations of total organic carbon (TOC) and total iodine  
62 (TI) of new particles were compared to evaluate the relative importance of organics and iodine in  
63 new particle growth. The identity and transformation mechanisms of organic compounds were  
64 identified to provide a more complete story of coastal NPF from low-tide macroalgal emission. Our

65 study is thus complementary to prior laboratory and field studies of I-NPF, but has an emphasis on  
66 organics.

## 67 2. Experiments

### 68 2.1 Experimental apparatus and sample collection

69 Similar to Potential Aerosol Mass (PAM) Oxidation Flow Reactor, a bag reactor was designed to  
70 provide an oxidizing environment for simulating atmospheric oxidation processes of algae-emitted  
71 VOCs. The bag reactor was made from 75  $\mu\text{m}$ -thick fluorinated ethylene propylene (FEP) Teflon  
72 (1.2 m $\times$ 1.5 m, flat dimension). The volume of the bag at full inflation was determined  
73 experimentally to be about 200 L. The bag was suspended vertically (Figure 1) and kept in the dark  
74 or directly exposed to room light of fluorescent lamp. Because the purpose of this study is to  
75 qualitatively measure the oxidation products of algae-emitted VOCs, wall loss, production rate and  
76 other kinetic factors in the bag reactor were not evaluated. Fresh macroalgae (*Undaria pinnatifida*)  
77 was collected from intertidal zone at Xiangshan gulf of east China coast and stored at -10  $^{\circ}\text{C}$  until the  
78 experiments. 2 kg macroalgae was put in a 20 L Pyrex glass bottle that was filled with  $\sim$ 1 L natural  
79 seawater. The specimens was partially exposed to the air to simulate tidal emersion of macroalgae. A  
80 flow of particle-free ultra high purity (UHP) air blew algae-emitted VOCs out of the bottle and  
81 merged with a diluting air flow before entering the bag reactor.

82 Two types of experiments were conducted. In the three ozonolysis experiments, ozone ( $\text{O}_3$ ) was  
83 generated by flowing an UHP air flow through a 5 Watts 185 nm UV lamp. The  $\text{O}_3$  flow was fed just  
84 before the bag reactor was fully inflated. Final  $\text{O}_3$  concentration in the bag reactor was measured to  
85 be  $\sim$ 200 ppbv using an ozone analyzer (Model 49i, Thermo-Fisher Scientific Inc.). In an additional  
86 OH-enhanced experiment, the  $\text{O}_3$ /VOC mixture flow was directed through a 254 nm UV light before  
87 entering the bag reactor. OH radicals were produced via the reaction  $\text{O}_3+h\nu\rightarrow\text{O}_2+\text{O}(^1\text{D})$  and  
88  $\text{O}(^1\text{D})+\text{H}_2\text{O}\rightarrow 2\text{OH}$ .

89 Before each experiment, the bag was purged for several hours to reduce background particle  
90 concentrations to below  $1\text{ cm}^{-3}$ . The bag reactor was first operated in a static mode to monitor the  
91 time evolution of gaseous products and particle size, and then in a dynamic mode to collect enough  
92 particles for offline chemical analysis. In the static mode, the bag was first filled to full inflation with  
93 the VOCs/ $\text{O}_3$  flows. The flows were then shut down; a Scanning Mobility Particle Sizer (SMPS,  
94 model 3936, TSI Inc., Shoreview, MN, USA) and an Aerodyne iodide-CIMS pulled two flows of 0.3  
95 liters per minute (lpm) and 1.8 lpm out of the bag, respectively. The SMPS measured the particle

96 number size distribution from 14 to 600 nm.

97 In the dynamic mode, the VOCs/O<sub>3</sub> flow of 3 lpm was fed to the bag continuously, while the  
98 SMPS and a vacuum pump (GAST Group Ltd.) pulled sample flows of 0.3 and 2.7 lpm, respectively,  
99 out of the bag reactor. This resulted in an overall residential time of 67 minutes for the O<sub>3</sub>/VOC  
100 mixture in the fully inflated bag. The particles in the 2.7 lpm sample flow were collected onto a  
101 Zefluor® PTFE membrane filter mounted in a filter inlet for gases and aerosols (FIGAERO) for  
102 iodide-CIMS analysis, or alternatively, onto 47 mm diameter double quartz fiber filter pack mounted  
103 in a filter holder for ESI-orbitrap MS, ICP-MS and TOC analysis. The front filter of the double filter  
104 pack collected the particles, while the back filter placed downstream of the front filter was supposed  
105 to adsorb the same amount of volatile species as the front filter.

## 106 **2.2 Chemical analysis**

107 Before the ozonolysis experiments, the algae-emitted VOCs in the bag reactor was collected by a  
108 6-liter pre-evacuated stainless-steel canisters (Entech Instruments, Inc., Simi Valley, CA, USA) and  
109 was analyzed using a quadrupole GC-MS system (model TH-300B, Wuhan Tianhong Instruments Co.  
110 Ltd., Wuhan, China). The algae-emitted VOCs, as well as their gaseous and particulate products,  
111 were also measured by the FIGAERO-iodide-CIMS. Iodide-adduct chemical ionization is well suited  
112 for measuring oxygenated or acidic compounds with minimal fragmentation. More details of the  
113 GC-MS and FIGAERO-iodide-CIMS measurements can be found in Supporting Material. The  
114 theory and design of the two instruments were described by Wang et al. (2014) and Lopez-Hilfiker et  
115 al. (2014).

116 The particles collected on quartz fiber filters were sent for offline quantification of TOC and TI,  
117 as well as non-target analysis of organic compounds using ESI-orbitrap MS. The front and back  
118 filters were treated, separately, following the procedure as below: the filter was ultrasonicated twice  
119 with 10-mL water and acetone nitrile solvent mixture (v:v=1:1). The extract was filtered by a 0.2 µm  
120 PTFE syringe filter and evaporated in a rotary evaporator to 0.5 mL. After being centrifuged for 30  
121 min at 12000 rpm, the supernatant was collected for TI analysis by Agilent 1100 HPLC-7900  
122 ICP-MS (Agilent Technologies, Santa Clara, CA, USA) and TOC analysis by a TOC analyzer  
123 (Model TOC-5000A, Shimadzu, Japan). TI or TOC in the particles was obtained by subtracting the  
124 amount on the back filter from that on the front filter. Nontarget analysis of organic compounds in  
125 the supernatant was conducted using a Q Exactive hybrid Quadrupole-Orbitrap mass spectrometer  
126 (Thermo Scientific, Bremen, Germany). The supernatant was directly infused by a syringe pump and  
127 ionized in negative ESI source. All the ions in the m/z range from 50 to 500 Th were scanned with a

128 mass resolution of 70000. The chemically sound CHO molecular formulas were computed with a  
129 mass tolerance of  $\pm 2$  ppm for these ions. Only the compounds that existed solely in the front filter or  
130 with ion intensity in the front filter higher than that in the back filter by a factor of 3 were regarded  
131 as the organic compounds in the particle phase.

### 132 **3. Results and discussion**

#### 133 **3.1 Relative mass contribution of organic carbon and iodine to new particles**

134 Typical banana-shape particle size spectrum observed in the static mode of an ozonolysis  
135 experiment is shown in Figure 2a. In the presence of room light, new particles larger than 14 nm  
136 were observed only 58 minutes after the injection of ozone flow. This relative long time is due to the  
137 build-up of O<sub>3</sub> concentration and subsequent accumulation of oxidation products. No particles were  
138 formed in the absence of room light or ozone. In the dynamic mode experiments, O<sub>3</sub> in the bag  
139 reactor was kept at its maximum concentration 200 ppbv. With a prolonged residential time of 67  
140 min, the particles grew to  $102 \pm 23$  nm, which was measured by the SMPS at the outlet of the bag  
141 reactor. The TOC and TI measurements show that organic compounds contributed more particle  
142 mass than iodine with TOC/(I+TOC) ratio of  $96.1 \pm 2.9\%$  (Table 1).

143 In the OH-enhanced experiment (dynamic mode), more particulate products were generated with  
144 enhanced oxidation capacity: TI in the particles increased by a factor of 10.8; TOC increased by a  
145 factor of 2.7; particle number concentration increased by a factor of 7.4. On the other hand, particle  
146 size decreased to 73 nm and TOC/(TI+TOC) ratio decreased to 92.9% (Table 1). These differences  
147 indicate that more iodine nuclei were produced with enhanced OH concentration, probably via  
148  $\text{OIO} + \text{OH} \rightarrow \text{HOIO}_2$  (Plane et al., 2006). Competitive uptake of condensing organic vapors onto these  
149 iodine nuclei limited the growth of individual new particles. Nevertheless, organic compounds  
150 overwhelmingly dominated over iodine in the mass contribution to new particle growth.

151 The significant organic contribution observed in the laboratory condition is generally consistent  
152 with TOC/(I+TOC) ratio of 98.2% in 10-56 nm new particles collected during a coastal I-NPF event in  
153 China (Yu et al., 2019), although TOC and TI during the field event are two orders of magnitude  
154 lower than those in the bag reactor (Table 1). Mean diameter of new particles was observed to be  
155 only 16 nm during the field event. But those small new particles are expected to grow into CCN  
156 active sizes, given longer residence time and uptake of more condensing vapors in the atmosphere.

## 157 **3.2 Macroalgal emission**

158 It is of particular interest to know what VOCs are emitted from coastal macroalgae. They are  
159 potential precursors of iodine particle nucleation and growth. The canister sampling followed by  
160 GC-MS analysis showed that the top 9 non-CHO compounds with highest TIC peak areas (Table 2)  
161 are C<sub>5</sub> alkanes, C<sub>10</sub> alpha-pinene and halogenated C<sub>1</sub>, C<sub>3</sub> and C<sub>5</sub> alkanes. The top 10 CHO  
162 compounds are C<sub>2</sub>-C<sub>6</sub> alcohols and carbonyls with saturated or unsaturated carbon chain.

163 Iodide-CIMS is more sensitive to more oxygenated or acidic compounds and thus complementary  
164 to the GC-MS measurement. The 76 organic precursors detected by iodide-CIMS before ozone  
165 addition were characterized by C<sub>1,2,3,6</sub> and O<sub>2-3</sub> formulas (Figure 3a). The top 7 compounds with  
166 highest ion intensities were CH<sub>2</sub>O<sub>2</sub>, C<sub>2</sub>H<sub>4</sub>O<sub>2</sub>, C<sub>3</sub>H<sub>6</sub>O<sub>3</sub>, C<sub>6</sub>H<sub>10</sub>O<sub>3</sub>, C<sub>2</sub>H<sub>6</sub>O<sub>2</sub>, C<sub>4</sub>H<sub>8</sub>O<sub>2</sub> and C<sub>6</sub>H<sub>12</sub>O<sub>3</sub>,  
167 which accounted for 82.5% of total ion intensity. They are C<sub>1</sub>-C<sub>6</sub> mono-carboxylic acids, hydroxyl  
168 carboxylic acids or oxo-carboxylic acids with 2 to 3 oxygen atoms (Table 2). Their carbon atom  
169 numbers are in general consistent with the VOCs detected by GC-MS.

170 Relatively high signals of HNO<sub>3</sub> were observed as NO<sub>3</sub><sup>-</sup> and HNO<sub>3</sub>I<sup>-</sup> before the addition of ozone  
171 to the bag reactor. Because HNO<sub>3</sub> and HNO<sub>2</sub> were also observed as deprotonated ions or I<sup>-</sup> clusters in  
172 the particle phase during the NPF, HNO<sub>3</sub> is also an important precursor of particle formation.

## 173 **3.3 Gaseous and particulate products**

### 174 **3.3.1 Inorganic molecules and radicals**

175 Being different from nitrate-CIMS, our iodide-CIMS did not detect nucleating clusters of iodine  
176 oxides or oxyacids after the addition of ozone. Instead, dozens of new inorganic molecules or  
177 radicals were observed as clusters with I<sup>-</sup>, NO<sub>3</sub><sup>-</sup> or deprotonated ions in the gas or particle phase  
178 (Figure 4). We grouped these species by elemental composition and investigated their role in the  
179 NPF by observing how their gaseous ion intensities evolved during the NPF event in the bag reactor  
180 (Figure 2b-2f).

181 1. Cl, I, Cl<sub>2</sub> and ClI in the gas phase: the intensities of I and Cl increased ca. 10 minutes before 14  
182 nm particles appeared and decreased as the particles grew up. Based on prior work of Burkholder et  
183 al. (2004); Jimenez et al. (2003); O'Dowd et al. (2004), we suggested the photolysis of CH<sub>2</sub>Cl<sub>2</sub>,  
184 CHBrCl, CH<sub>3</sub>I and C<sub>3</sub>H<sub>7</sub>I was the source of halogen atoms (e.g., CH<sub>3</sub>I+hν→CH<sub>3</sub>+I). There was a  
185 time lag of 20-25 minutes between the appearances of Cl and I and those of ClI and Cl<sub>2</sub>, which were  
186 probably from the recombination of Cl and I atoms.

187 2. IO<sub>2</sub>, IO, ClIO, INO<sub>2</sub> and ClNO<sub>2</sub> in the gas phase: these species showed a similar time series to I  
188 and Cl atoms. IO, IO<sub>2</sub> and ClIO could be from the reactions between I, ClI and O<sub>3</sub>. INO<sub>2</sub> is usually  
189 thought to form upon the reaction I+NO<sub>2</sub>+M →INO<sub>2</sub>+M (Saiz-Lopez et al., 2012). ClNO<sub>2</sub> was likely  
190 to form upon similar reaction between Cl and NO<sub>2</sub> in the bag reactor.

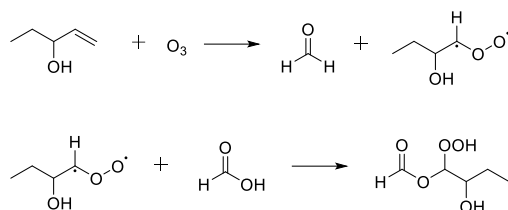
191 3. HIO<sub>3</sub> and INO<sub>3</sub>: the two species seem to be the end products of above intermediates, because  
192 their intensities kept on increasing during new particle growth. INO<sub>3</sub>, which is iodine nitrate IONO<sub>2</sub>,  
193 was detected in both gas and particle phases. IONO<sub>2</sub> probably formed upon the recombination of IO  
194 and NO<sub>2</sub> (IO+NO<sub>2</sub>+M→IONO<sub>2</sub>+M) (Saiz-Lopez et al., 2012). HIO<sub>3</sub> was likely to form via  
195 OIO+OH→HOIO<sub>2</sub> or I + H<sub>2</sub>O + O<sub>3</sub>→HOIO<sub>2</sub> + OH (Martín et al., 2020; Plane et al., 2006). HIO<sub>3</sub>  
196 was not detected in particle phase by iodide-CIMS, which is contrary to the observation by  
197 HPLC-ICP-MS that total iodine was mostly dominated IO<sub>3</sub><sup>-</sup> peak. The signals of IO<sup>-</sup>, IO<sub>2</sub><sup>-</sup> and  
198 HIONO<sub>3</sub><sup>-</sup> in the particle phase are therefore most likely to result from thermal decomposition of  
199 HIO<sub>3</sub> to HIO and HIO<sub>2</sub> in the FIGAERO thermal desorption process.

200 4. CH<sub>3</sub>SO<sub>3</sub>H, S<sub>2</sub><sup>-</sup>, S<sub>3</sub><sup>-</sup>, SO<sub>3</sub><sup>-</sup>: We observed methane sulfonic acid (CH<sub>3</sub>SO<sub>3</sub>H, MSA) in both gas and  
201 particle phases. Gaseous MSA increased in the beginning, but decreased after new particles appeared  
202 (Figure 2f). Apparently, our measurement suggested MSA contributed to the growth of new particles,  
203 but it is unknown if it also participated in nucleation. We suggested S<sub>2</sub><sup>-</sup>, S<sub>3</sub><sup>-</sup>, SO<sub>3</sub><sup>-</sup> ions observed in the  
204 particle phase were thermal decomposition products of MSA.

### 205 3.3.2 Gaseous organic products

206 After ozone addition, a gradual transformation from C<sub>1</sub>-C<sub>3</sub> precursors to C<sub>5</sub>-C<sub>8</sub> gaseous products  
207 was observed during the NPF process (Figure 2h). In the meanwhile, the oxygen atom number of the  
208 compounds increased from 2-3 to 4-7 (Figure 2g). The formation of compounds with more carbon  
209 atoms than the parent VOCs is unlikely in the gas phase, except bimolecular reactions of stabilized  
210 Criegee intermediates (SCIs) that typically form upon alkene ozonolysis. Similar to isoprene  
211 ozonolysis (Inomata et al., 2014; Riva et al., 2017), we propose the SCI addition mechanism can  
212 also explain the transformation observed in our case: (1) C<sub>4</sub> SCIs formed upon the ozonolysis of  
213 CHO precursors with C=C double bonds (e.g., those observed by GC-MS in Table 2). (2) the  
214 insertion of C<sub>4</sub> SCIs into carboxylic acid precursors (e.g., those observed by CIMS in Table 2)  
215 produced oligomeric hydroperoxides. An example was shown in Scheme I for the reactions of most  
216 abundant ethyl vinyl carbinol (C<sub>5</sub>H<sub>10</sub>O), ozone and formic acid (CH<sub>2</sub>O<sub>2</sub>), but the same mechanism is  
217 also applicable for ethyl vinyl ketone (C<sub>5</sub>H<sub>8</sub>O) and other abundant C<sub>2</sub>-C<sub>5</sub> carboxylic acids and  
218 hydroxyl carboxylic acids. As a result, a series of gaseous oligomeric hydroperoxides C<sub>5</sub>H<sub>10</sub>O<sub>5</sub>,

219 C<sub>6</sub>H<sub>10</sub>O<sub>5</sub>, C<sub>6</sub>H<sub>12</sub>O<sub>5</sub>, C<sub>7</sub>H<sub>12</sub>O<sub>6</sub>, C<sub>7</sub>H<sub>14</sub>O<sub>6</sub>, C<sub>8</sub>H<sub>14</sub>O<sub>5</sub>, C<sub>8</sub>H<sub>16</sub>O<sub>6</sub>, C<sub>8</sub>H<sub>16</sub>O<sub>5</sub> and C<sub>9</sub>H<sub>16</sub>O<sub>6</sub> were observed with  
220 high intensity by iodide-CIMS.



221

Scheme I

### 222 3.3.3 Particulate organic products

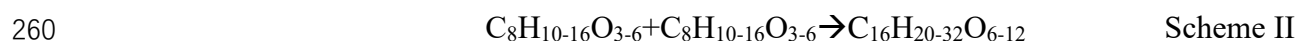
223 In the end of a typical ozonolysis experiment (dynamic mode), 100 and 364 new formulas were  
224 observed in the gas and particle phases, respectively, including 73 semi-VOCs appeared in both gas  
225 and particle phases. Those semi-VOCs accounted for 81 and 20% of total ion intensities of gaseous  
226 and particulate products, respectively. Being different from unimodal atom number distributions of  
227 gaseous products ( $C_{\max}=7$  and  $O_{\max}=5$ , Figure 3b), particulate products were characterized by  
228 distinct bimodal or trimodal distribution of carbon number ( $C_{\max}=8, 14$  and  $16$ , Figure 3c) and  
229 oxygen number ( $O_{\max}=4$  and  $8$ ), implying possible dimer formation via accretion reactions in the  
230 particle phase.

231 ESI-Orbitrap MS differs from FIGAERO-iodide-CIMS in extraction method (ultrasonic solvent  
232 extraction from quartz fiber filter *vs.* thermal desorption from PTFE membrane filter), ionization  
233 source (electrospray ionization *vs.* iodide-adduct chemical ionization) and MS resolving power  
234 (70000 *vs.* 4500). The result showed that ESI-orbitrap MS and FIGAERO-iodide-CIMS detected 336  
235 and 364 organic formulas, respectively, in the particle phase. 167 organic formulas were commonly  
236 observed by both methods, which accounted for 87% and 54% of total ion intensity of organic  
237 formulas by the two methods, respectively (Figure S1). As shown in Figure 3c and 3d,  
238 FIGAERO-iodide-CIMS had better sensitivity toward the organic compounds with more oxygen  
239 atoms (e.g.,  $O \geq 8$ ) and carbon atoms (e.g.,  $C \geq 10$ ). As a result, bimodal carbon and oxygen atom  
240 number distributions were observed by FIGAERO-iodide-CIMS, but not ESI-orbitrap MS.

241 The measurement by ESI-orbitrap MS provided more insights about the formation mechanism of  
242 particulate products. We compared the 336 formulas detected by ESI-orbitrap MS in our study with  
243 the 414 formulas of isoprene ozonolysis SOA products (Nguyen et al., 2010) and 922 formulas of  
244 alpha-pinene ozonolysis SOA products (Putman et al., 2012) measured by the ESI-orbitrap MS. It  
245 was found that 72% of the formulas in this study can also be found in isoprene SOA, but only 39%  
246 can be found in alpha-pinene SOA. This seems to imply that some similar alkene ozonolysis

247 reactions occurred in our system and isoprene ozonolysis.

248 For such a highly complex system full of various algae-emitted precursors, it is impossible to  
249 simply propose a reaction mechanism to explain the formation of all particulate products, nor to list  
250 all reactions occurring in the bag reactor. On the basis of particle-phase oligomer chemistry (Seinfeld  
251 and Pandis, 2016), especially the well-understood isoprene ozonolysis SOA chemistry (Inomata et al.,  
252 2014; Nguyen et al., 2010; Riva et al., 2017), we suggest a variety of accretion reactions without  
253 uniform oligomerization pattern (e.g., esterification, aldol condensation, hemiacetal reactions,  
254 peroxyhemiacetal formation and SCI reactions, etc.) transformed  $O_{\max}=4$  and  $C_{\max}=8$  multifunctional  
255 monomers (like alcohols, carbonyls, hydroperoxides, carboxylic acids) to  $O_{\max}=8$  and  $C_{\max}=14$  or 16  
256 dimers. Scheme II illustrated addition type self- and cross-oligomerization between  $C_6$  and  $C_8$   
257 monomers produces  $C_{14}$  and  $C_{16}$  dimers. All the formulas in Scheme II are among the most abundant  
258 ones observed in the particle phase by the iodide-CIMS.



#### 261 **4. Conclusions**

262 Using a suite of mass spectrometers, we reported, for the first time, the chemical compositions of  
263 volatile precursors emitted by real-world coastal macroalgae and their gaseous and particulate  
264 oxidation products. In the presence of room light and ozone, the photolysis of halogenated  $C_{1,3,5}$   
265 alkanes ends up as  $HIO_3$  and  $INO_3$ . It was most likely  $HIO_3$  initiated NPF and provided nuclei for the  
266 further condensation of other products like  $INO_3$ , MSA and CHO compounds. Gas-phase SCI  
267 reactions and particle-phase accretion reactions transformed  $C_1$ - $C_6$  and  $O_2$ - $O_3$  precursors gradually to  
268 particulate products with  $C_{\max}=8, 14$  and 16 and  $O_{\max}=4$  and 8. As a result, organic carbon were  
269 found to overwhelmingly dominated over iodine in the mass contribution to the new particle growth.  
270 Although our instruments did not allow the detection of nucleating clusters of iodine oxides or  
271 oxyacids, our study provided important complementary information to the ongoing laboratory and  
272 field researches of coastal I-NPF.

#### 273 **Data Availability Statement**

274 All data related to figures and tables in this study are archived and made available through  
275 Zenodo data repository <https://doi.org/10.5281/zenodo.6965859>.

276 **Acknowledgement**

277 This work was supported by the National Science Foundation of China (grant no. 41975831 and  
278 42175131) and Start-up research funding from China University of Geosciences.

279 **References**

- 280 Allan, J. D., et al. (2015), Iodine observed in new particle formation events in the Arctic atmosphere  
281 during ACCACIA, *Atmos. Chem. Phys.*, *15*(10), 5599-5609, doi:10.5194/acp-15-5599-2015.
- 282 Ashu-Ayem, E. R., U. Nitschke, C. Monahan, J. Chen, S. B. Darby, P. D. Smith, C. D. O'Dowd, D. B.  
283 Stengel, and D. S. Venables (2012), Coastal Iodine Emissions. 1. Release of I<sub>2</sub> by *Laminaria*  
284 *digitata* in Chamber Experiments, *Environmental Science & Technology*, *46*(19), 10413-10421,  
285 doi:10.1021/es204534v.
- 286 Baccarini, A., et al. (2020), Frequent new particle formation over the high Arctic pack ice by  
287 enhanced iodine emissions, *Nature Communications*, *11*(1), 4924,  
288 doi:10.1038/s41467-020-18551-0.
- 289 Beck, L. J., et al. (2021), Differing Mechanisms of New Particle Formation at Two Arctic Sites,  
290 *Geophysical Research Letters*, *48*(4), e2020GL091334, doi:<https://doi.org/10.1029/2020GL091334>.
- 291 Burkholder, J. B., J. Curtius, A. R. Ravishankara, and E. R. Lovejoy (2004), Laboratory studies of  
292 the homogeneous nucleation of iodine oxides, *Atmospheric Chemistry and Physics*, *4*(1), 19-34,  
293 doi:10.5194/acp-4-19-2004.
- 294 Donahue, N. M., et al. (2013), How do organic vapors contribute to new-particle formation?,  
295 *Faraday Discussions*, *165*(0), 91-104, doi:10.1039/C3FD00046J.
- 296 Ehn, M., et al. (2014), A large source of low-volatility secondary organic aerosol, *Nature*, *506*(7489),  
297 476-479, doi:10.1038/nature13032.
- 298 Faxon, C., J. Hammes, M. Le Breton, R. K. Pathak, and M. Hallquist (2018), Characterization of  
299 organic nitrate constituents of secondary organic aerosol (SOA) from nitrate-radical-initiated  
300 oxidation of limonene using high-resolution chemical ionization mass spectrometry, *Atmospheric*  
301 *Chemistry and Physics*, *18*(8), 5467-5481, doi:10.5194/acp-18-5467-2018.
- 302 He, X. C., et al. (2021), Role of iodine oxoacids in atmospheric aerosol nucleation, *Science*,  
303 *371*(6529), 589-595, doi:10.1126/science.abe0298.
- 304 Heard, D. E., et al. (2006), The North Atlantic Marine Boundary Layer Experiment(NAMBLEX).  
305 Overview of the campaign held at Mace Head, Ireland, in summer 2002, *Atmos. Chem. Phys.*, *6*(8),  
306 2241-2272, doi:10.5194/acp-6-2241-2006.
- 307 Huang, R.-J., et al. (2022), Heterogeneous iodine-organic chemistry fast-tracks marine new particle  
308 formation, *Proceedings of the National Academy of Sciences*, *119*(32), e2201729119,  
309 doi:10.1073/pnas.2201729119.
- 310 Inomata, S., K. Sato, J. Hirokawa, Y. Sakamoto, H. Tanimoto, M. Okumura, S. Tohno, and T.  
311 Imamura (2014), Analysis of secondary organic aerosols from ozonolysis of isoprene by proton  
312 transfer reaction mass spectrometry, *Atmospheric Environment*, *97*, 397-405,  
313 doi:<https://doi.org/10.1016/j.atmosenv.2014.03.045>.
- 314 Jimenez, J. L., R. Bahreini, D. R. Cocker III, H. Zhuang, V. Varutbangkul, R. C. Flagan, J. H.  
315 Seinfeld, C. D. O'Dowd, and T. Hoffmann (2003), New particle formation from photooxidation of  
316 diiodomethane (CH<sub>2</sub>I<sub>2</sub>), *Journal of Geophysical Research: Atmospheres*, *108*(D10),  
317 doi:<https://doi.org/10.1029/2002JD002452>.
- 318 Kundu, S., R. Fisseha, A. L. Putman, T. A. Rahn, and L. R. Mazzoleni (2012), High molecular  
319 weight SOA formation during limonene ozonolysis: insights from ultrahigh-resolution FT-ICR  
320 mass spectrometry characterization, *Atmos. Chem. Phys.*, *12*(12), 5523-5536,  
321 doi:10.5194/acp-12-5523-2012.

322 Kundu, S., R. Fisseha, A. L. Putman, T. A. Rahn, and L. R. Mazzoleni (2017), Molecular formula  
323 composition of  $\beta$ -caryophyllene ozonolysis SOA formed in humid and dry conditions, *Atmospheric*  
324 *Environment*, 154, 70-81, doi:<https://doi.org/10.1016/j.atmosenv.2016.12.031>.

325 Lopez-Hilfiker, F. D., et al. (2014), A novel method for online analysis of gas and particle  
326 composition: description and evaluation of a Filter Inlet for Gases and AEROSols (FIGAERO),  
327 *Atmospheric Measurement Techniques*, 7(4), 983-1001, doi:10.5194/amt-7-983-2014.

328 Martín, J. C. G., T. R. Lewis, M. A. Blitz, J. M. C. Plane, M. Kumar, J. S. Francisco, and A.  
329 Saiz-Lopez (2020), A gas-to-particle conversion mechanism helps to explain atmospheric particle  
330 formation through clustering of iodine oxides, *Nature Communications*, 11(1), 4521,  
331 doi:10.1038/s41467-020-18252-8.

332 McFiggans, G., et al. (2010), Iodine-mediated coastal particle formation: an overview of the Reactive  
333 Halogens in the Marine Boundary Layer (RHAMBLE) Roscoff coastal study, *Atmospheric*  
334 *Chemistry and Physics*, 10(6), 2975-2999, doi:10.5194/acp-10-2975-2010.

335 McFiggans, G., et al. (2004), Direct evidence for coastal iodine particles from Laminaria macroalgae  
336 – linkage to emissions of molecular iodine, *Atmos. Chem. Phys.*, 4(3), 701-713,  
337 doi:10.5194/acp-4-701-2004.

338 Monahan, C., E. R. Ashu-Ayem, U. Nitschke, S. B. Darby, P. D. Smith, D. B. Stengel, D. S. Venables,  
339 and C. D. O'Dowd (2012), Coastal Iodine Emissions: Part 2. Chamber Experiments of Particle  
340 Formation from Laminaria digitata-Derived and Laboratory-Generated I<sub>2</sub>, *Environmental Science*  
341 *& Technology*, 46(19), 10422-10428, doi:10.1021/es3011805.

342 Nguyen, T. B., A. P. Bateman, D. L. Bones, S. A. Nizkorodov, J. Laskin, and A. Laskin (2010),  
343 High-resolution mass spectrometry analysis of secondary organic aerosol generated by ozonolysis  
344 of isoprene, *Atmospheric Environment*, 44(8), 1032-1042,  
345 doi:<https://doi.org/10.1016/j.atmosenv.2009.12.019>.

346 O'Dowd, C. D., J. L. Jimenez, R. Bahreini, R. C. Flagan, J. H. Seinfeld, K. Hämeri, L. Pirjola, M.  
347 Kulmala, S. G. Jennings, and T. Hoffmann (2002), Marine aerosol formation from biogenic iodine  
348 emissions, *Nature*, 417, 632, doi:10.1038/nature00775.

349 O'Dowd, C. D., M. C. Facchini, F. Cavalli, D. Cebrunis, M. Mircea, S. Decesari, S. Fuzzi, Y. J. Yoon,  
350 and J.-P. Putard (2004), Biogenically driven organic contribution to marine aerosol, *Nature*, 431,  
351 676-680.

352 Plane, J. M. C., D. M. Joseph, B. J. Allan, S. H. Ashworth, and J. S. Francisco (2006), An  
353 Experimental and Theoretical Study of the Reactions OIO + NO and OIO + OH, *The Journal of*  
354 *Physical Chemistry A*, 110(1), 93-100, doi:10.1021/jp055364y.

355 Putman, A. L., J. H. Offenberg, R. Fisseha, S. Kundu, T. A. Rahn, and L. R. Mazzoleni (2012),  
356 Ultrahigh-resolution FT-ICR mass spectrometry characterization of  $\alpha$ -pinene ozonolysis SOA,  
357 *Atmospheric Environment*, 46, 164-172, doi:<https://doi.org/10.1016/j.atmosenv.2011.10.003>.

358 Riva, M., S. H. Budisulistiorini, Z. F. Zhang, A. Gold, J. A. Thornton, B. J. Turpin, and J. D. Surratt  
359 (2017), Multiphase reactivity of gaseous hydroperoxide oligomers produced from isoprene  
360 ozonolysis in the presence of acidified aerosols, *Atmospheric Environment*, 152, 314-322,  
361 doi:10.1016/j.atmosenv.2016.12.040.

362 Saiz-Lopez, A., J. M. C. Plane, A. R. Baker, L. J. Carpenter, R. von Glasow, J. C. Gómez Martín, G.  
363 McFiggans, and R. W. Saunders (2012), Atmospheric Chemistry of Iodine, *Chemical Reviews*,  
364 112(3), 1773-1804, doi:10.1021/cr200029u.

365 Saunders, R. W., and J. M. C. Plane (2005), Formation Pathways and Composition of Iodine Oxide  
366 Ultra-Fine Particles, *Environmental Chemistry*, 2(4), 299-303,  
367 doi:<https://doi.org/10.1071/EN05079>.

368 Seinfeld, J. H., and S. N. Pandis (2016), *Atmospheric chemistry and physics: from air pollution to*  
369 *climate change*, 3rd ed., John Wiley and Sons. Inc., New York.

370 Sellegri, K., et al. (2016), Evidence of atmospheric nanoparticle formation from emissions of marine  
371 microorganisms, *Geophysical Research Letters*, 43(12), 6596-6603,

372 doi:<https://doi.org/10.1002/2016GL069389>.

373 Sellegri, K., Y. J. Yoon, S. G. Jennings, C. D. O'Dowd, L. Pirjola, S. Cautenet, H. Chen, and T.  
374 Hoffmann (2005), Quantification of Coastal New Ultra-Fine Particles Formation from In situ and  
375 Chamber Measurements during the BIOFLUX Campaign, *Environmental Chemistry*, 2(4), 260-270,  
376 doi:<https://doi.org/10.1071/EN05074>.

377 Sipilä, M., et al. (2016), Molecular-scale evidence of aerosol particle formation via sequential  
378 addition of HIO<sub>3</sub>, *Nature*, *advance online publication*, doi:10.1038/nature19314  
379 [http://www.nature.com/nature/journal/vaop/ncurrent/abs/nature19314.html#supplementary-informati](http://www.nature.com/nature/journal/vaop/ncurrent/abs/nature19314.html#supplementary-information)  
380 [on](http://www.nature.com/nature/journal/vaop/ncurrent/abs/nature19314.html#supplementary-information).

381 Wang, M., et al. (2020), Photo-oxidation of Aromatic Hydrocarbons Produces Low-Volatility  
382 Organic Compounds, *Environmental science & technology*, 54(13), 7911-7921,  
383 doi:10.1021/acs.est.0c02100.

384 Wang, M., et al. (2014), Development and validation of a cryogen-free automatic gas chromatograph  
385 system (GC-MS/FID) for online measurements of volatile organic compounds, *Analytical Methods*,  
386 6(23), 9424-9434, doi:10.1039/C4AY01855A.

387 Whitehead, J. D., G. B. McFiggans, M. W. Gallagher, and M. J. Flynn (2009), Direct linkage  
388 between tidally driven coastal ozone deposition fluxes, particle emission fluxes, and subsequent  
389 CCN formation, *Geophysical Research Letters*, 36(4), doi:doi:10.1029/2008GL035969.

390 Yan, C., et al. (2020), Size-dependent influence of NO(x) on the growth rates of organic aerosol  
391 particles, *Science advances*, 6(22), eaay4945, doi:10.1126/sciadv.aay4945.

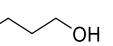
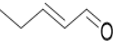
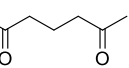
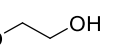
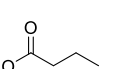
392 Yu, H., L. Ren, X. Huang, M. Xie, J. He, and H. Xiao (2019), Iodine speciation and size distribution  
393 in ambient aerosols at a coastal new particle formation hotspot in China, *Atmospheric Chemistry*  
394 *and Physics*, 19(6), 4025-4039, doi:10.5194/acp-19-4025-2019.

395

Table 1. Particle number concentration ( $N$ ), mean diameter ( $D_p$ ), total organic carbon (TOC) and total iodine (TI) of new particles with a residential time of 67 min in the bag reactor in the ozonolysis experiments and OH-enhanced experiment (dynamic mode). Those of 10-56 nm new particles collected by a nano Micro-Orifice Uniform Deposit Impactor (nano-MOUDI, MSP, Inc.) during an I-NPF event at a coastal site of Ningbo, China (Yu *et al.*, 2019) were also listed.

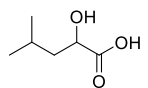
	TOC ( $\mu\text{g m}^{-3}$ )	TI ( $\mu\text{g m}^{-3}$ )	TOC/(TI+TOC)	$N$ ( $\text{cm}^{-3}$ )	$D_p$ (nm)
ozonolysis experiments	45.6 $\pm$ 9.7	0.88 $\pm$ 0.34	96.1 $\pm$ 2.9%	(5.58 $\pm$ 2.04) $\times$ 10 <sup>4</sup>	102 $\pm$ 23
OH-enhanced experiment	125.3	9.5	92.9%	4.16 $\times$ 10 <sup>5</sup>	73
I-NPF event at a coastal site of China	0.7	0.0135	98.2%	6.00 $\times$ 10 <sup>5</sup>	16

Table 2. Major volatile organic compounds emitted by macroalgae as potential NPF precursors, sorted by TIC peak area measured by GC/MS or MS peak intensity measured by iodide-CIMS

	Formula	Structure	Peak area/MS peak intensity
1	C <sub>5</sub> H <sub>12</sub>		1.90×10 <sup>6</sup>
2	C <sub>5</sub> H <sub>10</sub>		1.59×10 <sup>6</sup>
3	CH <sub>3</sub> I		1.37×10 <sup>6</sup>
4	C <sub>3</sub> H <sub>7</sub> I		7.60×10 <sup>5</sup>
5	CHBr <sub>3</sub>		4.71×10 <sup>5</sup>
6	C <sub>5</sub> H <sub>11</sub> I		3.75×10 <sup>5</sup>
7	CHBr <sub>2</sub> Cl		2.71×10 <sup>5</sup>
8	CH <sub>2</sub> Cl <sub>2</sub>		2.55×10 <sup>5</sup>
9	C <sub>10</sub> H <sub>16</sub>		2.26×10 <sup>5</sup>
1	C <sub>2</sub> H <sub>6</sub> O		1.70×10 <sup>7</sup>
2	C <sub>3</sub> H <sub>6</sub> O		1.38×10 <sup>7</sup>
3	C <sub>4</sub> H <sub>6</sub> O <sub>2</sub>		1.30×10 <sup>7</sup>
4	C <sub>6</sub> H <sub>12</sub> O		1.03×10 <sup>7</sup>
5	C <sub>5</sub> H <sub>10</sub> O		1.00×10 <sup>7</sup>
6	C <sub>4</sub> H <sub>10</sub> O		5.16×10 <sup>7</sup>
8	C <sub>2</sub> H <sub>4</sub> O		3.46×10 <sup>7</sup>
9	C <sub>6</sub> H <sub>10</sub> O		2.88×10 <sup>7</sup>
7	C <sub>5</sub> H <sub>8</sub> O		1.45×10 <sup>7</sup>
10	C <sub>4</sub> H <sub>8</sub> O		1.37×10 <sup>7</sup>
1	CH <sub>2</sub> O <sub>2</sub>		1.58×10 <sup>6</sup>
2	C <sub>2</sub> H <sub>4</sub> O <sub>2</sub>		9.52×10 <sup>5</sup>
3	C <sub>3</sub> H <sub>6</sub> O <sub>3</sub>		9.21×10 <sup>5</sup>
4	C <sub>6</sub> H <sub>10</sub> O <sub>3</sub>		4.44×10 <sup>5</sup>
5	C <sub>2</sub> H <sub>6</sub> O <sub>2</sub>		2.88×10 <sup>5</sup>
6	C <sub>4</sub> H <sub>8</sub> O <sub>2</sub>		1.17×10 <sup>5</sup>

7

$C_6H_{12}O_3$



$1.12 \times 10^5$

---

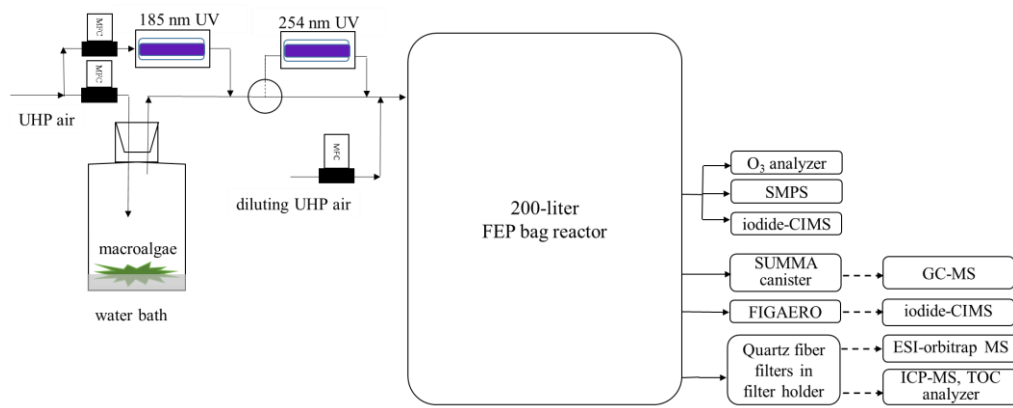


Figure 1. Schematic of experimental setup. Solid line: air flows. Dashed lines: sent for offline chemical analysis.

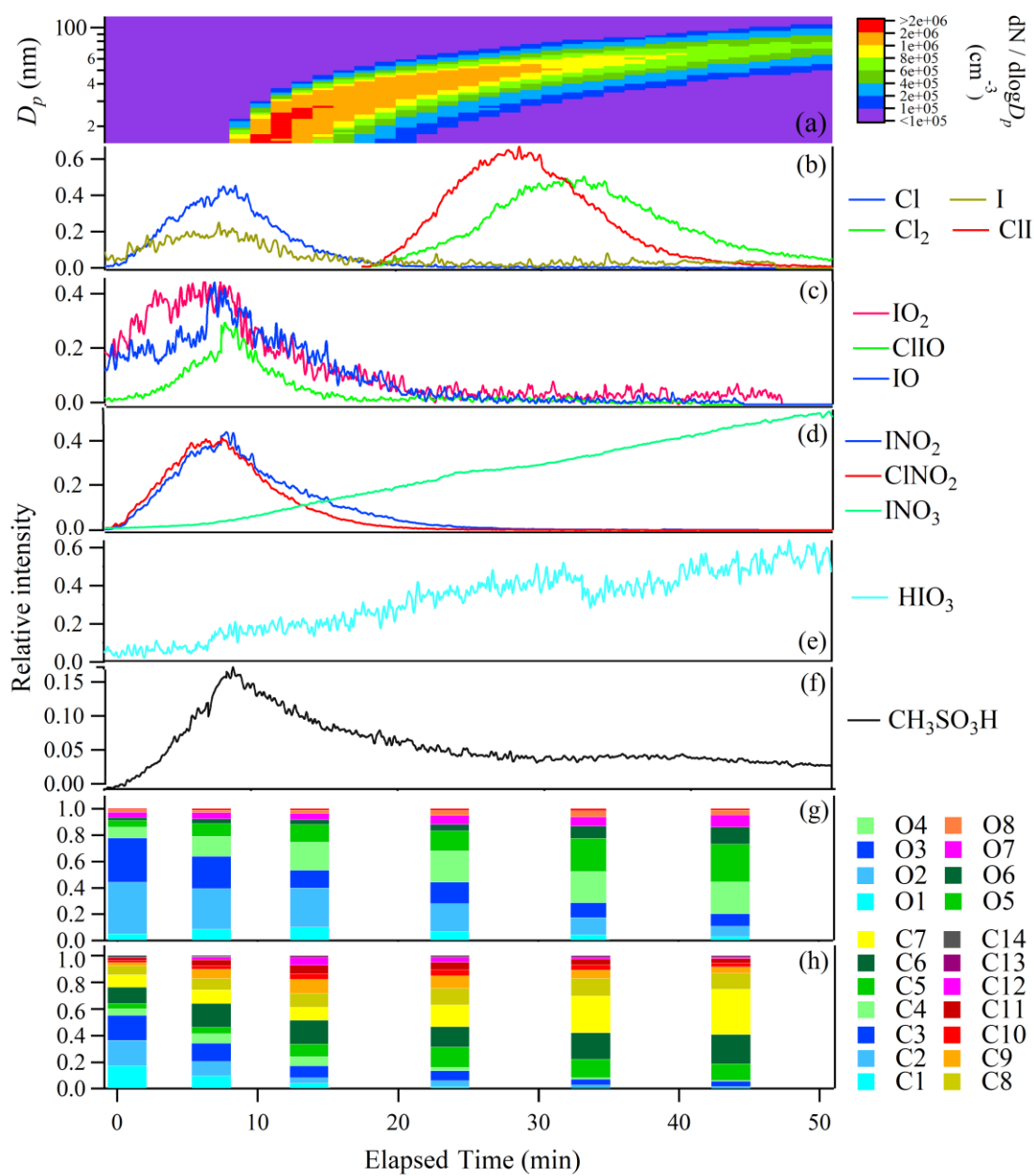


Figure 2. Time evolution of particle number size distribution (a) and relative intensities of gaseous molecules and radicals (b-f); the fractions of organic compounds grouped by O and C atom numbers in the selected time points (g-h) in a typical ozonolysis experiment (static mode). Time zero was chosen as the start time when HIO<sub>3</sub> was observed.

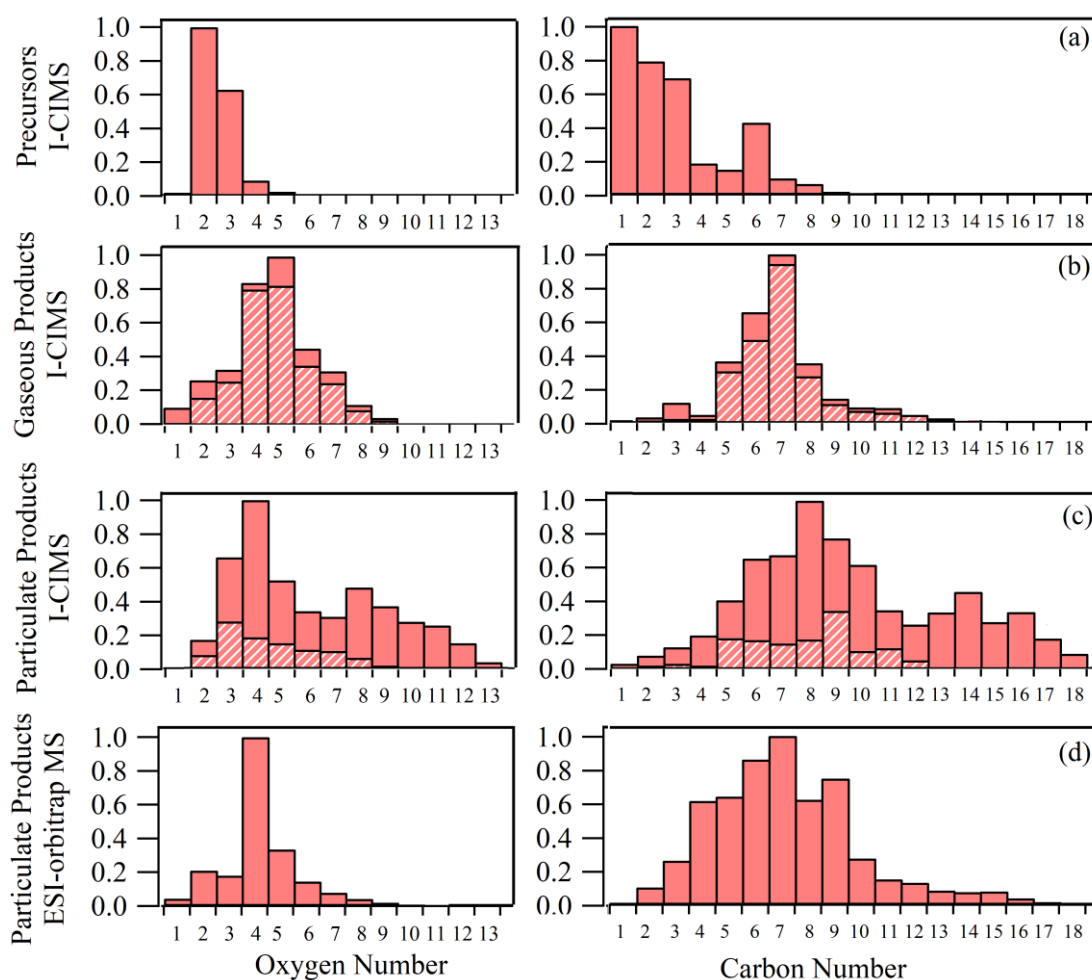


Figure 3. Oxygen and carbon atom number distributions of potential VOC precursors (a), gaseous products (b) and particulate products measured by iodide-CIMS (c), as well as the particulate products measured by ESI-orbitrap MS (d) in a typical ozonolysis experiment (dynamic mode). Hatched bars indicate the fractions of organic formulas observed in both gas and particle phases by iodide-CIMS.

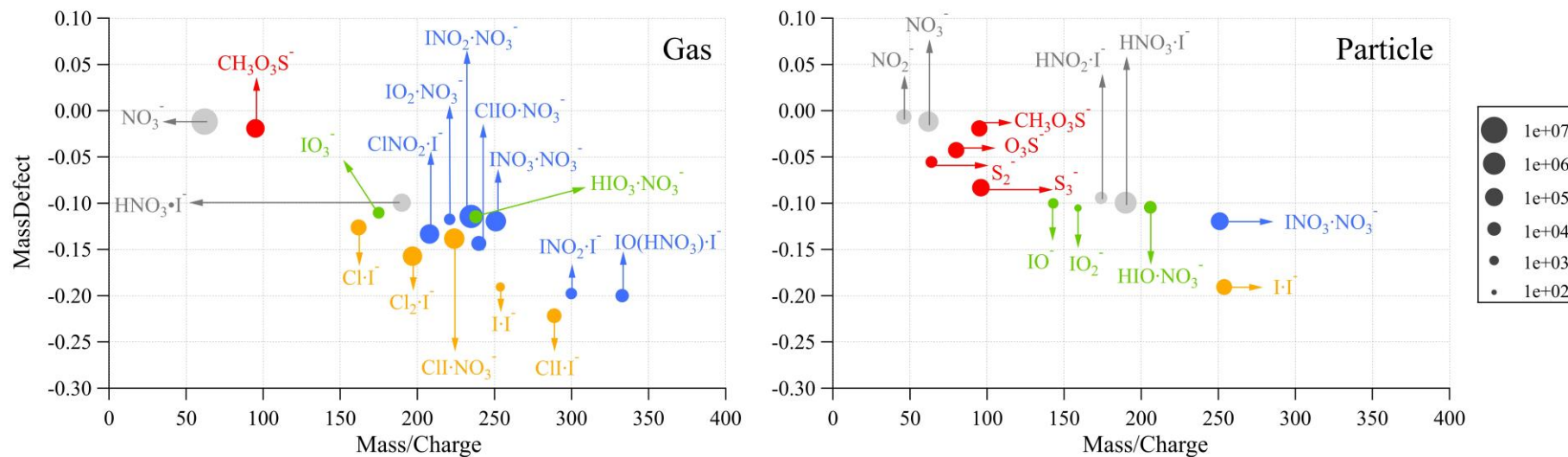


Figure 4. Integrated ion intensities of inorganic molecules and radicals in the gas phase (static mode) and particle phase (dynamic mode) measured by iodide-CIMS in a typical ozonolysis experiment. The ions were coded in color according to their elemental composition